ELSEVIER

Contents lists available at ScienceDirect

Molecular Catalysis

journal homepage: www.journals.elsevier.com/molecular-catalysis





Influence of oxidizing and reducing pretreatment on the catalytic performance of CeO₂ for CO oxidation

Kyung-Min Lee ^a, Melanie Brito ^a, Jamie DeCoster ^a, Kelvin Linskens ^a, Kareem Mehdi ^a, Won-Il Lee ^a, Emily Kim ^b, Hajoon Kim ^c, Gihan Kwon ^d, Chang-Yong Nam ^{a,e}, Taejin Kim ^{a,*}

- ^a Department of Materials Science and Chemical Engineering, Stony Brook University, Stony Brook, NY 11794, USA
- ^b Hankuk Academy of Foreign Studies, Yongin, Gyeonggi-do KS009, South Korea
- ^c Radnor Senior High School, Radnor, PA 19087, USA
- ^d National Synchrotron Light Source II, Brookhaven National Laboratory, Upton, NY 11973, USA
- e Center for Functional Nanomaterials, Brookhaven National Laboratory, Upton, NY 11973, USA

ARTICLE INFO

Keywords:
Cerium oxide
Pretreatment temperature effect
CO oxidation
Physical property

ABSTRACT

Cerium oxide (CeO₂) and ceria-based materials have been extensively investigated as catalyst and support materials for various catalytic reactions, due to higher oxygen storage capacity and excellent redox properties. In the current work, we investigated the impact of pretreatment conditions (e.g., oxidation and reduction) on the physical properties of bulk CeO₂ and catalytic activity for CO oxidation as a model reaction. To understand the physical properties of pretreated CeO₂ catalysts, a suite of complementary characterization techniques, including X-ray diffraction (XRD), surface area analysis (BET), X-ray photoemission spectroscopy (XPS), and Raman spectroscopy, were applied. The results showed that a higher pretreatment temperature led to a decreased specific surface area (SSA), a decrease in oxygen vacancy/defect sites, and increased crystallite size, while surface $\text{Ce}^{3+}/\text{Ce}^{4+}$ ratio did not show a specific relationship to the treatment conditions. The 700 °C treated CeO₂ samples under oxidizing and reducing conditions showed higher specific oxidation rate (μ mol_{CO}/s/m²) compared to other samples at 280 and 300 °C (or < 15% CO conversion). The CO conversion per total mass of catalysts, however, decreased with increasing temperatures, especially at 700 °C under reducing condition, indicating that the catalytic performance was affected by the physical properties (SSA, oxygen vacancy/defect sites, and crystallite size)..

1. Introduction

The carbon monoxide (CO) oxidation reaction with metal and metal oxide catalysts has been of great interest for a variety of practical applications, such as three-way catalytic converters, fuel cells, and gas sensors [1–4]. Traditionally, supported platinum group metals (PGMs) have been investigated for CO oxidation. While these catalysts have seen widespread use since their development by I. Langmuir, they still suffer from low catalytic activity at temperatures below 100 °C, especially when compared to gold-based catalysts such as those created by Lin et al. [5–7]. In addition to the surface species, supports have also affected the CO oxidation reaction. Germani et al. have developed catalysts that incorporate oxides such as alumina and ceria to improve the low-temperature performance of PGM catalysts [8].

There has been a wide range of research on the surface pretreatment

of many metal oxides catalysts, especially oxidation and reduction pretreatments. Yang et al. performed an oxidation–reduction pretreatment on ${\rm Co_3O_4/Al_2O_3}$ catalysts leading to surface reconstruction that decreased crystallite size and exposed more ${\rm Co^{3^+}}$ that increased catalytic activity [9]. Bumajdad et al. studied effect of oxidizing pretreatment at different temperature with a- ${\rm Cr_2O_3}$ catalysts and results indicates that samples pretreated at lower temperatures (400 °C) exhibited better catalytic properties due to smaller particle sizes and larger surface areas when compared to samples treated at higher temperatures (600 or 800 °C) [10]. Additionally, Bueno et al. found that subjecting ${\rm SnO_2}$ to oxidative conditions gave smaller crystallite sizes than as-received samples [11]. Lovell et al. utilized a reduction-oxidation–reduction (ROR) pretreatment method on Ni-SiO₂ catalysts and found that the pretreatment led to decreased Ni deposit sizes and an altered interaction between the Ni and SiO₂ thus allowing for improved

E-mail address: taejin.kim@stonybrook.edu (T. Kim).

^{*} Corresponding author.

catalytic performance [12]. Jang et al. utilized an oxidation–reduction pretreatment on Ni $_3$ Al foils which allowed for a Ni layer to form on the surface of the foil thus enabling improved catalytic activity [13]. From these studies, the wide array of surface changes and thus catalytic activity changes that can occur due to pretreatment, such as oxidation, reduction, and combined oxidation–reduction, are highlighted. These results emphasize the need to examine the impact of oxidation and reduction pretreatments on CeO $_2$ as the interaction between the pretreatment and the pure CeO $_2$ may not be completely inferred from the results of other metal oxides. Especially since CeO $_2$ has been investigated as a support material, understanding how physiochemical properties of CeO $_2$ change under oxidation and reduction pretreatments may allow an improved understanding of ceria-supported catalysts and their property changes due to pretreatments.

Among the several support materials, ceria has been used extensively due to its high redox property and formation of oxygen vacancies [14–16]. In general, the oxygen vacancies are formed when cerium ions reduce from their 4+ to 3+ state; these vacancies increase the number of catalytic active sites on the ceria surface, which, in turn, leads to higher catalytic activity [17–19]. Several authors investigated CO oxidation over CeO_2 supported Au catalysts using the density functional theory and concluded that oxygen vacancies create Ce^{3+} , which increases the O_2 adsorption on the Au- Ce^{3+} site and provides a new CO oxidation pathway [20–22]. The catalytic activity of ceria supported catalysts are also related to the exposed ceria crystalline planes. Recently, W. Wang et al. studied the effect of ceria faces on CO oxidation over Cu/CeO_2 catalysts [23]. The authors reported that CeO_2 -{110} prevent the formation of Cu(I) active sites, resulting in low CO oxidation activity, while Cu(I) formation was feasible on CeO_2 -{111} surfaces.

Previous studies have examined the impact of surface pretreatments on ceria using oxidizing conditions, but very few have utilized reducing conditions. E. Aneggi et al. studied the effect of oxygen treatment of ceria on CO oxidation activity and reported that high treatment temperatures (>500 °C) decrease catalytic activity, although other variables (i.e., oxygen vacancy) and treatment conditions (i.e., reducing) were not considered [24]. The authors claimed that exposing the active {100}-type surface at high temperatures is directly related to the high specific reaction rate, while the surface area was decreased with increasing calcination temperatures. Wang et al. studied ceria thin films at elevated temperatures under oxidizing conditions to examine the impact of this type of pretreatment on the physical structure of the ceria [25]. The author found that increasing temperature resulted in increased average grain size and concentration of Ce³⁺. However, they did not examine the relationship between the physical properties and catalytic activity. Although well-shaped model ceria (i.e., nanosphere, octahedra, nanorod) samples have been continuously studied to understand the facet-activity relationship [24,26,27], ceria pretreatment effects on physical properties and their catalytic activity relationship require further evaluation, especially under reducing conditions due to the fact that defect site concentration, crystallite size, and surface area have critical impacts on the catalytic activity.

The present study is focused on the impact of pretreatment (oxidation and reduction) at broad ranges of temperature on the physical properties of CeO_2 catalysts and on the catalytic performance for CO oxidation as a model reaction. The structural changes were examined by several characterization techniques (i.e., UV-Raman, Visible-Raman, Brunauer-Emmet-Teller (BET) surface area measurement, X-ray photoelectron spectroscopy (XPS), and X-ray powder diffraction (XRD)), and the catalytic activity for CO oxidation of the samples was determined using a gas chromatograph (GC).

2. Experimental section

2.1. Catalyst synthesis

The ceria (HSA 5, Rhodia) catalysts were treated under different

conditions (oxidation and reduction). For the oxidized ceria samples, ceria powders were calcined for 6 h in air (Airgas, dry air, 20% oxygen and 80% nitrogen) at different temperatures (400, 500, and 700 °C) in a combustion boat with a tube furnace (Lindberg/Blue Mini-Mite, Thermo). The oxidized samples were denoted as CeO₂-400Oxi, CeO₂-500Oxi, and CeO₂-700Oxi. In the case of reduced CeO₂ catalysts, ceria powders were reduced in a H₂ flow (5% H₂ balanced with N₂, total flow rate of 50 ml min $^{-1}$) at 400, 500, and 700 °C for 3 h. The reduced samples were denoted as CeO₂-400R, CeO₂-500R, and CeO₂-700R. The temperature range was selected as it was found that oxygen vacancies begin to form at 500 °C, corresponding with surface vacancies forming, while 700 °C reduction temperature is correlated with oxygen vacancies forming in the bulk ceria [24,28].

2.2. Characterization

The specific surface area (SSA) and pore size of the catalysts were obtained by Micromeritics ASAP 1010 and calculated using the multipoint Brunauer-Emmett-Teller (BET) and Barrett-Joyner-Halenda (BJH) methods, respectively. For pretreatment, catalysts were degassed under vacuum for 4 h at 300 °C to remove volatiles and impurities. To determine molecular structures, UV-Raman and Visible-Raman spectra of the as-received and treated samples were obtained using Renishaw inViaTM Raman microscope (325 nm) and Horiba XploRATM Raman spectrometer (532 nm), respectively. For both Raman spectra, the acquisition time was 10 s, and the final spectrum was obtained after accumulation of 30 scans. X-ray diffraction (XRD) patterns were obtained by loading the powder samples in polyimide tubes that were then sealed with clay. The National Synchrotron Light source 28-ID-1 beamline (74.53 keV, $\lambda = 0.16635$ Å) was used to obtain the diffraction patterns. Dioptas was used to obtain one-dimensional X-ray diffraction (XRD) pattern from the two-dimensional XRD pattern [29]. The elemental compositions and oxidation state of prepared samples were characterized by X-ray photoelectron spectroscopy (XPS) on a custom-built XPS system equipped with a hemispherical electron energy analyzer (SPECS) and Al Ka X-ray source (1486.6 eV, SPECS).

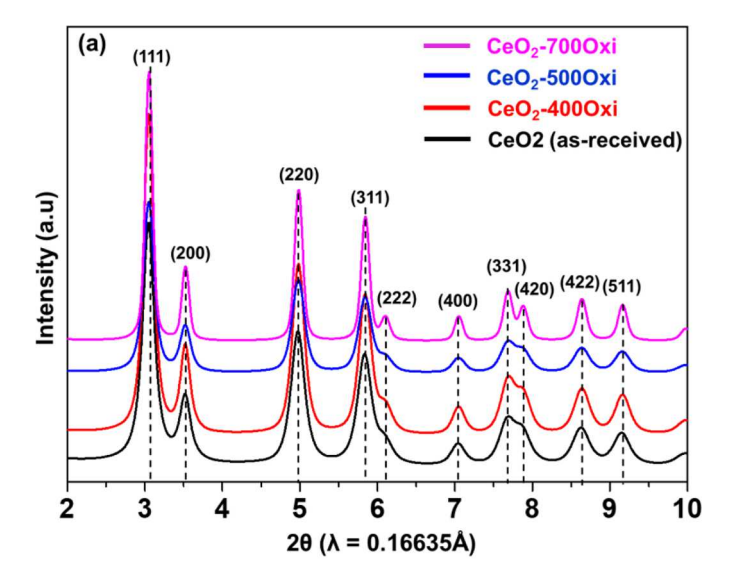
2.3. Catalytic activity test

To test the catalytic activity of the ceria samples, gas phase reactions were conducted in a fixed bed quartz reactor (OD 9.6 mm, ID 7 mm). The reactor was packed with 40 mg of the sieved (425 μm size sieve, Fisherbrand) catalyst powder which was held in place by quartz wool. Prior to reaction, the prepared catalysts were pretreated in He (30 ml min $^{-1}$) at 400 °C for 30 min with ramping rate of 10 °C min $^{-1}$. For CO oxidation, the gas mixtures were 4% CO (20 ml min $^{-1}$, 10% CO with He balance) and 4% O2 (2 ml min $^{-1}$, UHP grade) with He balance (28 ml min $^{-1}$, UHP grade) with a total flow rate of 50 ml min $^{-1}$. The reaction temperature was increased up to 500 °C at a ramping rate of 1 °C min $^{-1}$. During the process, a K-type thermocouple (Omega) was used to measure temperature and a mass flow meter (SLA5800 Series, Brooks Instrument) was used to measure the flow rates. The products of the reaction were analyzed with the TRACE $^{\rm TM}$ 1300 GC (Thermo Scientific) containing a capillary column (Carboxen® 1010 PLOT) and a TCD detector.

3. Results and discussion

3.1. Powder X-ray diffraction (XRD)

To determine the crystalline structure of the ceria samples, synchrotron XRD was employed. As shown in Fig. 1, the XRD patterns of samples are well defined indicating that the ceria samples are highly crystalline. The XRD patterns of all samples showed peaks at 2θ values 3.0° , 3.5° , 5.0° , 5.8° , 7.0° , 7.7° , 8.6° , and 9.1° that correspond to the (111), (200), (220), (311), (400), (331), (422), and (511) planes in fluorite structures of CeO₂, respectively [30,31]. For 400 and 500 °C



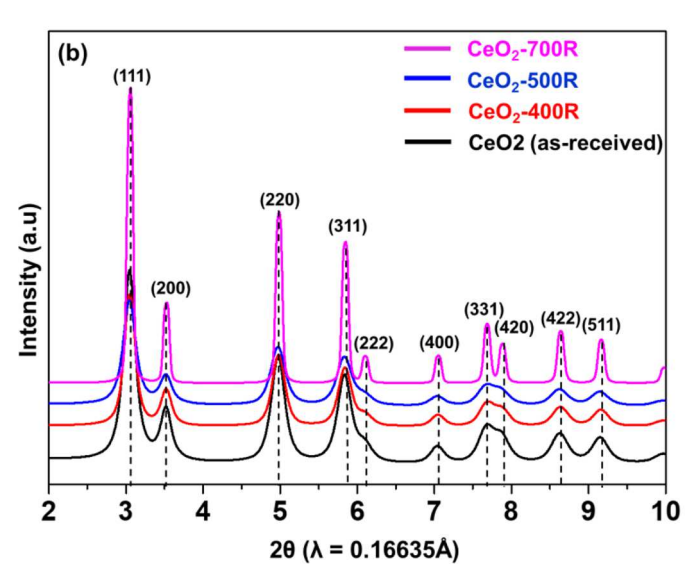


Fig. 1. XRD patterns of (a) ${\rm CeO_2}$ (as-received) and oxidized ${\rm CeO_2}$, (b) ${\rm CeO_2}$ (as-received) and reduced ${\rm CeO_2}$.

treated samples under oxidizing and reducing conditions, the XRD peak intensity and shape of the peaks were very similar to the as-received CeO_2 . In the case of 700 °C treated samples, however, it is clearly seen that the peaks became sharper with increasing peak intensity, indicating the change of crystallinity of CeO_2 with increasing treatment temperature to 700 °C [32]. Furthermore, new peaks appeared at 6.1° and 7.9° that can be attributed to the (222) and (420) planes respectively [30, 31].

The average crystallite sizes and lattice parameter of the cubic fluorite CeO_2 samples were determined based on the (111) peak using the Scherrer equation. As shown in Table 1, the full width half maximum (FWHM) and crystallite size of the 400 °C and 500 °C treated samples were very similar to the CeO_2 (as-received) sample, indicating that the crystalline CeO_2 structure was not affected by the treatment conditions (oxidizing and reducing). In the case of 700 °C treated samples under oxidizing and reducing conditions, however, FWHM and crystallite size were noticeably decreased and increased, respectively, while the lattice parameter was not changed. These results could be explained by the thermodynamic stability of the ceria. As reported by Berent et al., with increasing calcination temperature, there is an enhancement of the ratio of crystalline volume to surface area, which reduces the Gibbs free energy [33]. A lower Gibbs free energy is indicative of a more stable

Table 1 Peak position, full width half maximum (FWHM) of the peak, and the calculated crystallite size and lattice parameter of the CeO_2 (as-received) and treated CeO_2 samples.

Sample	Peak Position (°)	FWHM (°)	Crystallite size (nm)*	Lattice parameter (Å)**
CeO ₂ (as- received)	3.05	0.17	5.1	5.41
CeO ₂ -400Oxi	3.05	0.15	5.7	5.41
CeO ₂ -500Oxi	3.05	0.16	5.4	5.41
CeO ₂ -700Oxi	3.05	0.11	7.6	5.41
CeO ₂ -400R	3.05	0.16	5.3	5.41
CeO ₂ -500R	3.05	0.17	5.0	5.41
CeO ₂ -700R	3.06	0.09	10.1	5.40

*:
$$D(\mathring{A}) = \frac{k\lambda}{\beta \cdot \cos\theta}$$
 **: $a = \sqrt{h^2 + k^2 + l^2} \cdot d_{111} = \sqrt{3}d_{111}, \ d_{111} = \frac{\lambda}{2 \cdot \sin\theta_{111}}$ where, D

is the crystallite size, k is the shape factor (0.9), λ is the X-ray wavelength (0.16635 Å), β is the FWHM in radians of the $\mathrm{CeO_2}(111)$ peak, θ in radians is the Bragg angle of the peak, a is lattice parameter, and d is the spacing of (111) lattice planes.

material; as the treatment temperature increases, it transforms the material into a more stable form, hence the reason for the larger crystallite size. The increase of the crystallite size in the 700 °C treated samples is also indicative that the crystallinity was increased with increasing treatment temperature [34]. Furthermore, sintering of the material at high temperature could lead to larger crystallites forming [32]. Both the ratio of increased crystalline volume to surface area and the larger crystallite size indicated sintering of the material and a decrease in the surface area [32–34]. Comparing CeO₂-700R and CeO₂-700Oxi, the reduced sample shows a larger crystallite size than that of oxidized one. This result shows that sintering of CeO₂ sample could be enhanced under the reducing condition at higher treatment temperatures. The detailed physical properties of the CeO₂ relationship with the treatment conditions are discussed in the following sections.

3.2. Physical properties of the catalysts

To determine the physical properties of the prepared catalysts, such as specific surface area (SSA), total pore volume, and average pore size, BET analysis was employed, and results are listed in Table 2. For all treated samples, the SSA decreased with increasing temperature, while the pore volume showed similar results. When the pretreatment temperature was increased to 700°C, the SSA of the catalysts was drastically decreased for both the oxidized and reduced samples. This is most likely due to increased sintering of the particles at the higher temperatures combined with the change in oxidation states of bulk CeO₂ [35]. Both Wang et al. and Aneggi et al. showed similar results when examining the effect of increasing calcination temperatures on the surface area of CeO₂ catalysts [24,35]. Wang et al. found that the surface area of the ceria substrate composite catalysts was decreased as the calcination temperature increased, due to sintering of the samples and larger crystalline grains [35]. Aneggi et al. synthesized three different types of polycrystalline ceria powder and found that pore diameter increased, and surface area decreased with increasing calcination temperature due to sintering of ceria [24]. Comparing the SSA of the CeO₂-700R with the CeO_2 -7000xi sample, the 700R sample's SSA (29 m²/g, ~13% of the as-received CeO2 SSA) was much lower than that of 700Oxi SSA (79 m^2/g , ~37% of the as-received CeO₂ SSA). This result suggests that the reduction pretreatment at 700 °C results in more sintering due to the reduced oxygen species in the lattice, which is well matched to the XRD results. The average pore size was increased with increasing pretreatment temperature for the oxidized and reduced samples, due to blocking of the mesoporous structure and sintering effect [24,35]. In the case of the 7000xi (3.3 nm) and 700R (10.3 nm) samples, the average pore size was ~2 times and ~7 times bigger than that of the as-received CeO₂

Table 2
Specific surface area, total pore volume, average pore size, isotherm type, hysteresis loop range, and hysteresis loop type of bulk CeO₂ catalysts under oxidation and reduction pretreatment.

Sample	Specific surface area (m ² /g)	Total pore volume (cm ³ /g)	Average Pore Size (nm)	Isotherm Type	Hysteresis Loop Type
CeO ₂ (as-received)	216	0.16	1.6	IV	H1
CeO ₂ -400Oxi	212	0.17	1.6	IV	H1
CeO ₂ -500Oxi	201	0.18	1.8	IV	H1
CeO ₂ -700Oxi	79	0.16	3.3	V	НЗ
CeO ₂ -400R	210	0.18	1.6	IV	H1
CeO ₂ -500R	174	0.18	1.9	IV	H1
CeO ₂ -700R	29	0.14	10.3	V	Н3

(1.5 nm), respectively. The pore size distribution of the oxidized and reduced CeO_2 samples is shown in Fig. S2. The pore size distribution of the as-received, 400, and 500 °C treated samples showed a narrow distribution profile, while the 700 °C samples possessed a broad (less well-defined) pore size distribution profile, due to slit-shaped pore structure. Based on the XRD, SSA, and average pore size results, it could be concluded that reduction pretreatment, especially at 700 °C, results in more sintering of the particles than the oxidation pretreatment.

Fig. 2 shows the N₂ absorption-desorption isotherms of the asreceived and pretreated CeO2 samples. The isotherm curves show that the as-received, 400, and 500 °C treated samples exhibited a type IV isotherm with H1 hysteresis loop, representing the mesoporous structures and defined cylindrical pores [36-38]. The 7000xi and 700R samples exhibited a type V isotherm with an H3 hysteresis loop, which showed that they contained a more porous structure with slit-shaped pores that require a pressure much closer to the saturation pressure of the bulk fluid to undergo capillary condensation [39]. These results are consistent with the results for average pore size as the pretreatment temperature of 700 °C led to a significant decrease in SSA and an increase in pore size. This increase in pore size disrupts the capillary condensation process as a greater pressure needs to be applied for condensation to occur in the larger and less defined pores, and the hysteresis starts very close to a relative pressure of 1. In the case of the other samples and the as-received samples, the pores are much smaller, and that is seen in the hysteresis behavior as the vapor begins condensing at only 71% of the saturation pressure of the bulk fluid.

3.3. Raman spectroscopy

Raman spectroscopy, which is a type of vibrational spectroscopy, was utilized to measure lattice oscillations in the ceria and to understand molecular structure [40]. UV Raman spectra show four characteristic peaks at about 457–462 cm $^{-1}$, 600 cm $^{-1}$, 800 cm $^{-1}$, and 1180 cm $^{-1}$ which correspond to the cubic fluorite structure (F $_{2g}$), oxygen vacancy or defect sites (D), oxygen absorption, and the second-order longitudinal

optical (2LO) band, respectively (Fig. 3) [41,42]. The F_{2g} peak is caused by the vibration of the tetrahedrally arranged oxygen which are symmetrically oriented around the center of the unit cell [39]. As the treatment temperature increased to 700 °C, the F_{2g} peak became sharper and narrower, which could be indicative of increasing crystallinity [43]. In addition to the changing of peak shapes, at 700 °C, the F_{2g} peak was slightly shifted from 457 to 462 cm⁻¹ (blue-shift). The peak shift with increasing temperature was also clearly observed using the visible Raman spectrometer. As shown in Fig. S1 (a) and (b), the F_{2g} peak was shifted from 456 cm⁻¹ (as-received) to 468 cm⁻¹ (CeO₂-7000xi) or 466 cm⁻¹ (CeO₂-700R). Fig. S1 also showed that the F_{2g} peak of all samples increased in intensity and narrowed as the temperature increased. T. Hattori et al. reported that the F_{2g} peak is very sensitive to disorder of oxygen in the lattice, showing that increased treatment temperature under oxidizing conditions led to a blue shift and sharpened peaks [44]. It was also reported that the blue shift of the F_{2g} band could be caused by the deficiency of Ce³⁺ species and increasing of particle size [45–49]. Based on the result of the F_{2g} peak shift and literature, it can be hypothesized that the treated CeO2 sample at 700 °C should contain the lowest overall oxygen defect sites. The presence of a shoulder peak at 487 cm⁻¹ for ceria (Fig. 3(a) and (b)) can be attributed to distortion of the lattice [45].

In the case of D band, the peak positions (600 cm^{-1}) were not shifted under oxidizing (Figs. 3(a) and S1(a)) and reducing (Figs. 3(b) and S1 (b)) conditions, and the peak intensity of 7000xi and 700R samples was lower than that of other samples. To better understand the oxygen defects on catalysts, the ratio of the UV-Raman peak intensity of the D band and F_{2g} band (I_D/I_{F2g}) was evaluated. As shown in Table 3, the defect ratio for the oxidized and reduced samples decreased as the treatment temperature increased. In the case of 400 °C (CeO₂-4000xi and CeO₂-400R) or 500 °C (CeO₂-5000xi and CeO₂-500R) samples, the I_D/I_{F2g} ratios are similar at oxidizing and reducing conditions, indicating that treatment temperature is more critical compared to the gas compositions used for treatment (i.e., hydrogen or oxygen). The I_D/I_{F2g} ratios of CeO₂-7000xi and CeO₂-700R samples, however, are changed by both the

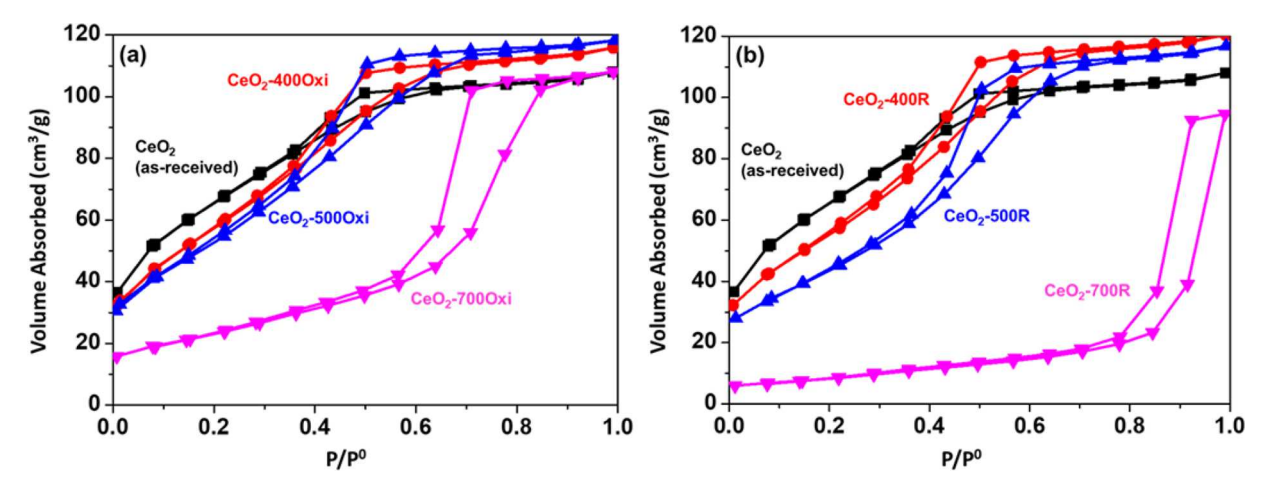
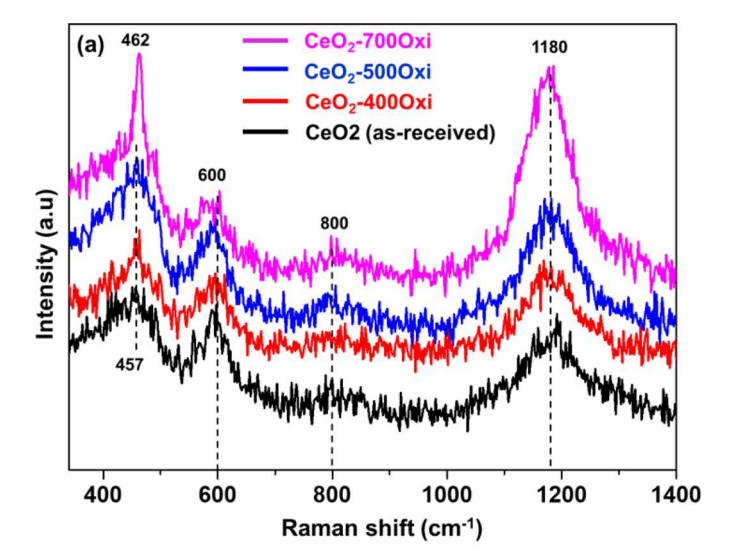


Fig. 2. N₂ adsorption-desorption isotherms of the (a) CeO₂ (as-received) and oxidized CeO₂, (b) CeO₂ (as-received) and reduced CeO₂.



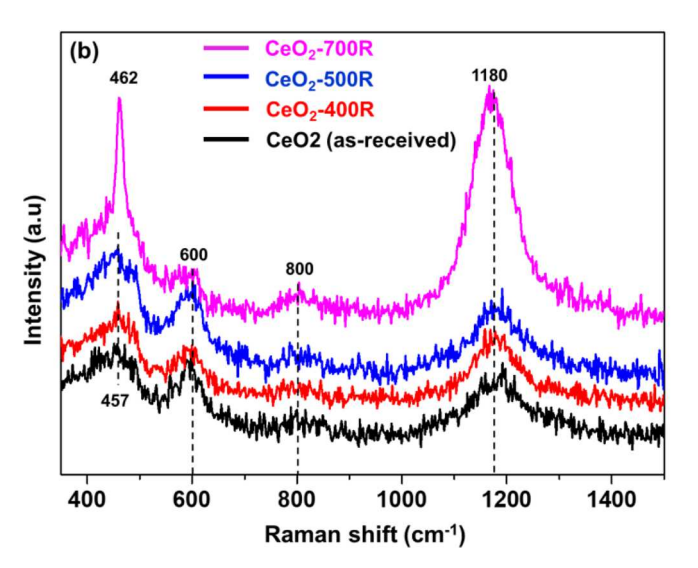


Fig. 3. UV Raman spectra of (a) CeO_2 (as-received) and oxidized CeO_2 , (b) CeO_2 (as-received) and reduced CeO_2 catalysts.

Table 3Defect ratio for oxidized, and reduced samples at different temperatures from UV Raman spectrographs.

Sample	Defect ratio (I_D/I_{F2g})		
CeO ₂ (as-received)	1.06		
CeO ₂ -400Oxi	0.82		
CeO ₂ -500Oxi	0.65		
CeO ₂ -700Oxi	0.30		
CeO ₂ -400R	0.82		
CeO ₂ -500R	0.66		
CeO ₂ -700R	0.16		

treatment temperature and gasses, suggesting both a temperature and gas composition effect. Since the I_D/I_{F2g} ratios are related to the defect sites in ceria, the relative defect concentrations of samples follow the sequence: CeO $_2$ (as-received) > CeO $_2$ -400Oxi and CeO $_2$ -400R > CeO $_2$ -500Oxi and CeO $_2$ -500> CeO $_2$ -700Oxi > CeO $_2$ -700R. Based on the XRD, BET, and Raman spectroscopy data, it is concluded that physical properties of CeO $_2$ were directly affected by the treatment temperatures.

3.4. X-ray photoelectron spectroscopy (XPS)

To determine the oxidation states and surface compositions of the samples, XPS analysis was employed. The XPS spectra of Ce 3d for the asreceived, oxidized, and reduced CeO2 samples were shown in Fig. 4. Fig. 4(a) and (b) show the deconvoluted Ce 3d spectra of the as-received, oxidized, and reduced CeO2 samples. The Ce 3d spectrum consists of two regions (3d_{3/2} and 3d_{5/2}) which are assigned to u and v bands, respectively, in the binding energy range of 878-920 eV: ten sub-peaks have been deconvoluted in the Ce 3d spectra. Four sub-peaks v_0 , v', u_0 , and u'(dark shades) could be assigned to Ce³⁺ species, while the other six sub peaks, v, v'', v''', u, u'', and u''', are related to Ce⁴⁺ [50,51]. The relative surface compositions of Ce³⁺ of prepared samples were calculated from deconvoluted XPS results and are summarized in Table 4. The relative contents of Ce³⁺ of the pretreated samples (both oxidized and reduced) showed similar results, but higher values than those of the as-received sample. These results suggest that the thermal pretreatment can promote the generation of surface Ce³⁺ species. However, the trends of XPS results do not match to the trends of defect ratio from the UV-Raman results. Since the UV-Raman is not only a surface technique, but also takes into account the bulk information, the defect ratio (I_D/I_{E2\sigma}) from UV-Raman results inferred that the higher treatment temperature affects the amount of defect sites in bulk of the material as well as the surface defect sites. Wu et al. reported that the D band from UV-Raman is most likely due to Frenkel-type oxygen vacancies instead of Ce³⁺ related vacancies [52]. Frenkel-type oxygen vacancies form on the surface and then move into the bulk of the ceria, so surface techniques such as XPS are not able to measure this type of oxygen vacancy. Although the amount of surface Ce³⁺ species is not directly related to defect ratio (I_D/I_{F2g}) from UV-Raman, we can possibly obtain the information for both surface and bulk defect sites or oxygen vacancies. Considering UV-Raman and XPS results, the higher pretreatment temperature led to decrease in bulk defect sites/oxygen vacancies, while surface Ce³⁺species increased after thermal pretreatment.

3.5. Catalytic activity testing

To understand the effect of the different pretreatment conditions on the catalytic performance, CO oxidation was performed as a model reaction. Fig. 5 exhibits the CO conversion as a function of reaction temperature over the oxidized and reduced CeO2 catalysts. For comparison purposes, the CO conversion for as-received CeO2 is also included. With increasing reaction temperature, the CO conversion increased; the CO conversion was negligible up to ~ 200 °C. In the case of oxidized CeO₂ catalysts, the 4000xi sample's CO conversions is very similar to that of as-received CeO2, while the 500Oxi and 700Oxi samples show a slightly lower CO conversion comparatively. In the case of the reduced samples, with increasing reduction temperature, the catalytic performance was decreased, while the 400R sample's CO conversion is similar to that of the as-received CeO₂. To compare the catalytic performance of the samples, T50 (reaction temperature for 50% CO conversion) was used and the values are shown in Fig. 5(a) and (b). The pretreatment effect on the CO oxidation over CeO2 catalysts shows the following trend: CeO2 (as-received), CeO_2 -400R, CeO_2 -400Oxi > CeO_2 -500R, CeO_2 -500Oxi > CeO₂-700Oxi >> CeO₂-700R. These results suggest that overall CO oxidation catalytic performance decreased with increasing treatment temperature, especially at 700 °C under reducing condition. To understand the contribution of surface area to the specific catalytic activity, the specific oxidation rate of as-received, oxidized, and reduced samples has been examined at 280 and 300 $^{\circ}\text{C}$ under the reaction kinetic regime (i.e., conversion < 15%). As shown in Fig. 6, the specific oxidation rate for the oxidized and reduced samples increased as the treatment temperature increased. In the case of the 400 °C (CeO2-400Oxi and CeO2-400R) and 500 °C (CeO₂-5000xi and CeO₂-500R) samples, the specific rate showed relatively similar results compared to the as-received sample's specific rate. When the pretreatment temperature was

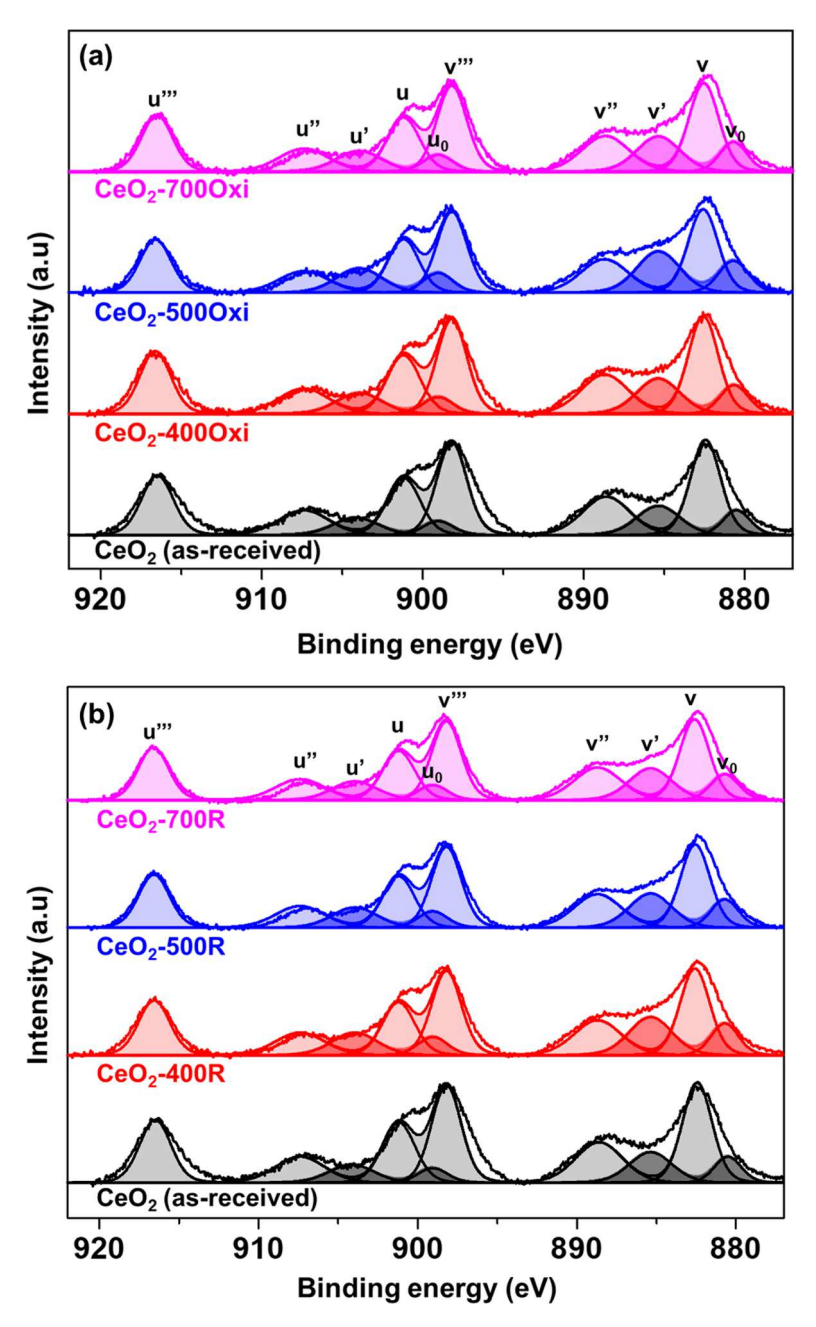


Fig. 4. Deconvoluted Ce 3d XPS spectra of (a) as-received and oxidized CeO2 and (b) as-received and reduced CeO2 samples.

Table 4Relative surface compositions of Ce³⁺ of prepared samples.

Sample	Atomic ratio (%) $Ce^{3+}/(Ce^{3+}+Ce^{4+})$
CeO ₂ (as-received)	20.17
CeO ₂ -400Oxi	23.02
CeO ₂ -500Oxi	29.11
CeO ₂ -700Oxi	24.96
CeO ₂ -400R	26.74
CeO ₂ -500R	25.36
CeO ₂ -700R	24.54

increased to 700 $^{\circ}$ C, however, the specific rate of the catalysts was drastically increased for both oxidized and reduced samples. It has been reported that the stability (less reactive) of surfaces of CeO_2 can be ordered as (111) < (100) < (110) [53,54]. Furthermore, Aneggi et al.

found that the reactive surface planes, such as (110) and (100), become visible after thermal treatment (calcination) [24]. Therefore, increased specific activity and decreased overall conversion could be explained by exposure of more reactive surfaces of (100) and (110) crystal planes with increasing treatment temperature accompanied by a decrease in the specific surface area.

3.6. Pretreatment effect on the physical properties and catalytic activity

The pretreatment (oxidation/reduction) of heterogeneous catalyst can have several effects on the physical properties and further affect the catalytic performance. Based on the XRD, BET and Raman results, the most apparent change resulting from the different pretreatments was the change in the 700 °C treated samples, especially the 700R sample. It has been reported that bulk CeO2 showed two reduction peaks at 400–500 °C and 750–800 °C, which ascribed to the reduction of surface (400–500 °C) and bulk or lattice (750–800 °C) oxygen species [38,55,

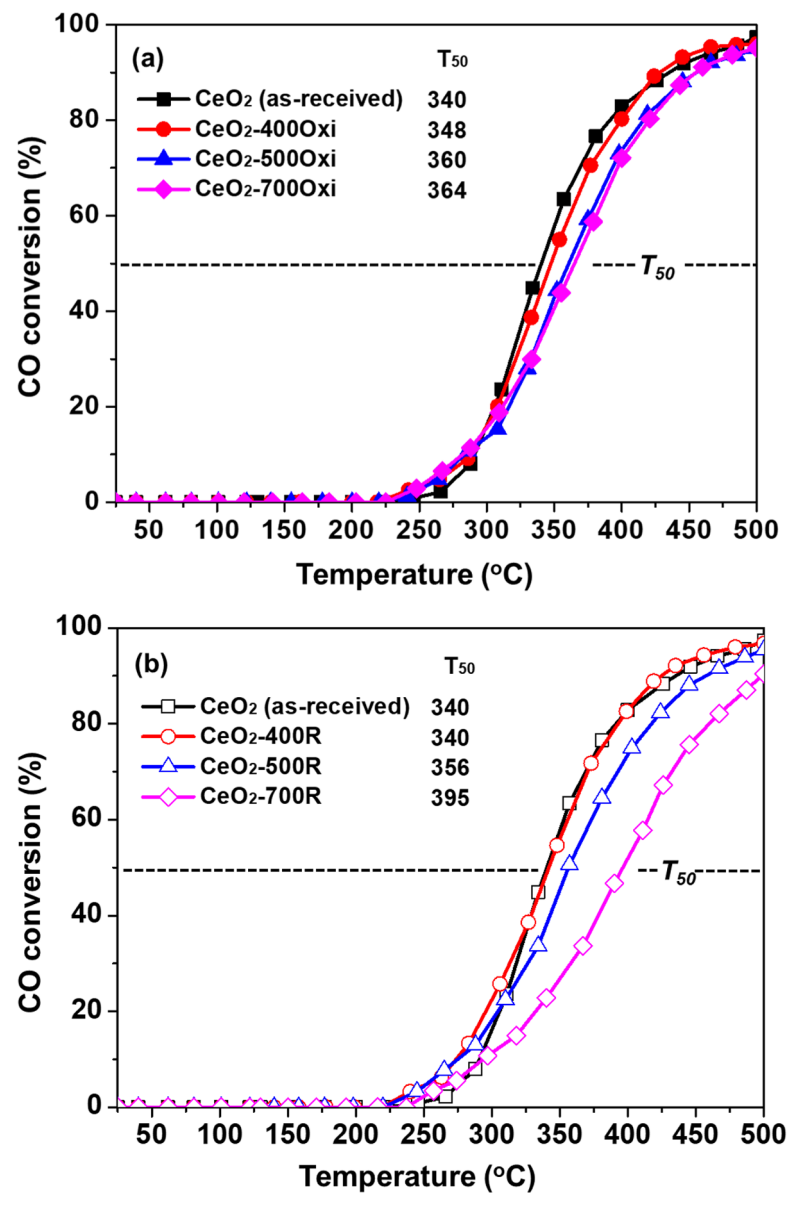


Fig. 5. CO conversion of (a) CeO₂ (as-received) and oxidized CeO₂, (b) CeO₂ (as-received) and reduced CeO₂.

56]. Based on the reported reduction temperatures of CeO2, it can be expected that the changes in physical properties, such as decrease in SSA and increase in pore size, of both oxidized and reduced CeO₂ samples is closely related to the reduction of oxygen species. To be specific, in the XRD patterns for both the oxidized and reduced samples, there was an increase in the crystallite size from about 5 nm to 7 nm and 10 nm for the oxidized and reduced samples, respectively (Fig. 1 and Table 1). This change also came with an increase in the peak intensity and a narrowing of the peak, indicating that the crystallinity of CeO₂ was increased with increasing treatment temperature. This increase in crystallinity was also observed in the Raman results as the peaks became narrower and more intense (Fig. S1). The higher crystallinity and increased crystallite size at higher treatment temperature was most likely caused by the sintering of the material [32]. These observations also agree with the BET results (Fig. 2 and Table 2). The SSA of the as-received, 400, and 500 °C samples, showed relatively similar results, but there is a large decrease in the surface area following the 700 °C pretreatment for both the oxidized and reduced samples. It has been reported that Raman spectroscopy can provide the formation of defective sites and oxygen vacancies on ceria structure [36,45,47,52,57–59]. Most previously published papers report

the defect site with the I_D/I_{F2g} ratios using visible Raman spectroscopy. Although the visible Raman spectroscopy is more popular compared to the UV-Raman spectroscopy, to study the oxygen vacancies, UV-Raman could be applied due to its higher surface sensitivity as compared to visible-Raman (Figs. 3 and S1). Guo et al. studied the oxygen vacancies on the surface of rare-earth doped ceria materials and concluded that surface oxygen vacancies can be easily detected using by UV laser [59]. The authors also reported that more bulk information (or F_{2g} Raman peak) with the visible Raman could be observed due to the weaker absorption of the visible laser. Based on the UV-Raman spectroscopy results (Fig. 3 and Table 3), the defect ratio (ID/IF2g) linearly decreased with increasing pretreatment temperatures, although it becomes much lower after the 700 $^{\circ}\text{C}$ pretreatment for both the oxidation and reduction pretreatments. This indicates that the most significant changes occur in the material after the 700 °C treatment, which is consistent with the XRD and BET results. Fig. 7 shows the trends of CeO₂ crystallite size, Raman peak intensity ratio ($I_{\text{D}}/I_{\text{F2g}}\text{),}$ and specific surface area (SSA) for the as-received, oxidized, and reduced CeO2 catalysts. It is clearly shown that the pretreatment (oxidation/reduction) at high temperature (700 °C) resulted in larger crystallite size (lower Gibbs free energy), low

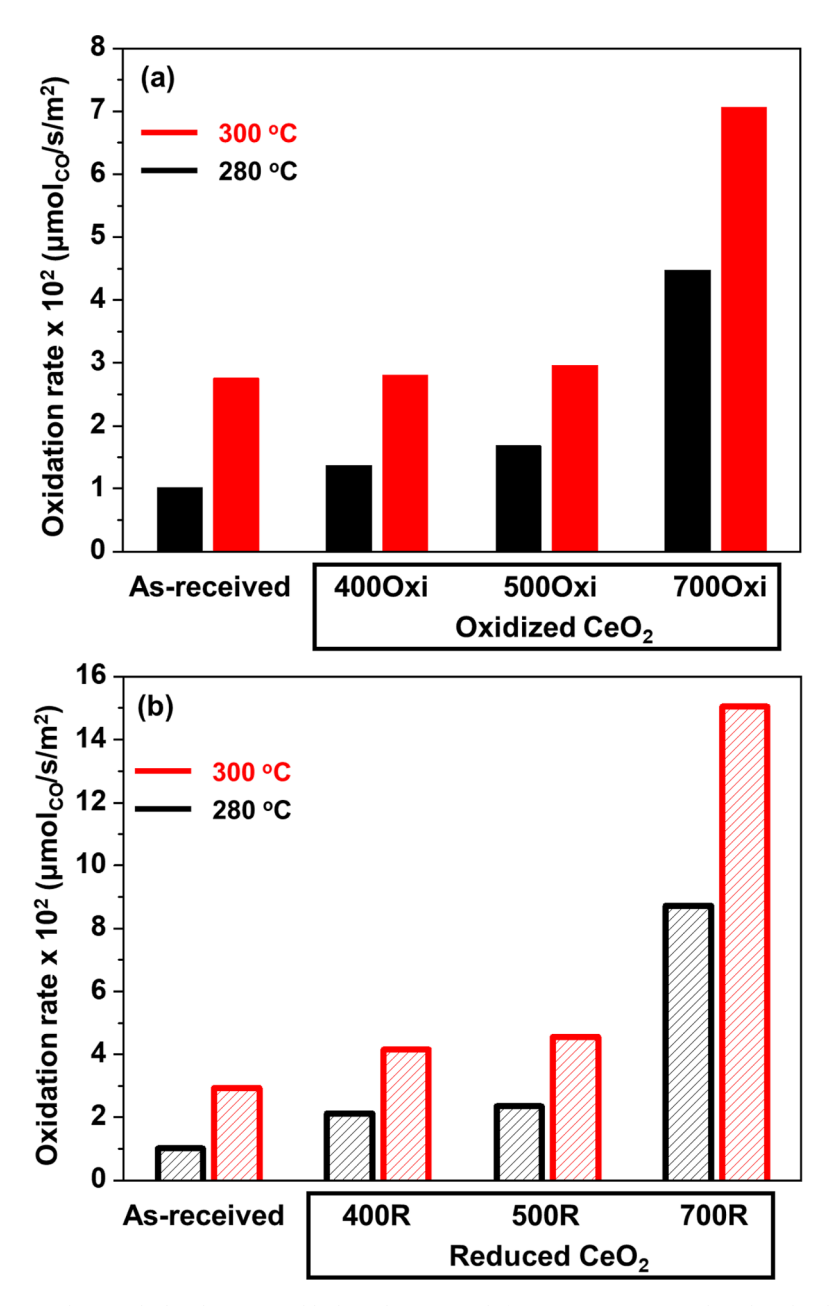


Fig. 6. Specific oxidation rate of CO oxidation calculated at 280 $^{\circ}$ C (black) and 300 $^{\circ}$ C (red) for (a) CeO₂ (as-received) and oxidized CeO₂, (b) CeO₂ (as-received) and reduced CeO₂.

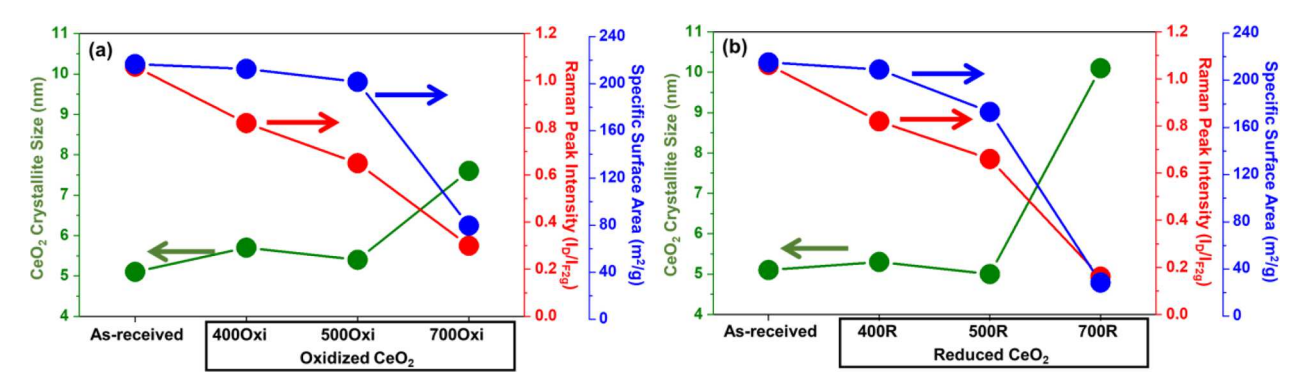


Fig. 7. The relationship between the CeO_2 crystallite size, Raman peak intensity ratio (I_D/I_{F2g}), and Specific surface area (SSA) of the as-received, oxidized, and reduced CeO_2 catalysts.

SSA (blockage of mesopores and sintering effect), and decreased defect ratio (oxygen vacancies/defect sites).

As discussed above, the pretreatment conditions (oxidation/reduction and temperatures) were directly related to the physical properties of the synthesized catalysts. From the catalytic activity results, it was shown that the CeO2 catalysts pretreated at lower temperatures showed better catalytic performance, with the oxidized samples having slightly higher conversion than the reduced samples. Fig. 8 (a-f) shows the relationship between catalytic performance (T₅₀ for CO conversion) and physical properties (i.e., specific surface area, crystallite size of CeO2 and Raman peak intensity (ID/IF2G)) of the as-received, oxidized, and reduced CeO2 catalysts. As shown in Fig. 8(a) and (b), the catalytic activity was decreased (or increasing of T50) with decreasing SSA, although the effect of relatively lower treatment temperatures (\leq 500 °C) on T₅₀ was trivial. In the case of 7000xi and 700R samples, however, it is clear that high treatment temperature with decreasing SSA directly affects the catalytic activity. The trends of catalytic activity are similar to the trends of CeO2 crystallite size for both the oxidized and reduced catalysts in that the change is negligible at lower temperatures before showing a significant increase for the 700 °C samples (Fig. 8(c) and (d)). In the case of T_{50} vs defect ratio (I_D/I_{F2g}) , the catalytic activity was decreased with decreasing defect ratio which is well matched to the reported results (Fig. 8(e) and (f)). Based on physical properties and catalytic activity results, the catalytic performance for CO oxidation is directly related to the oxygen vacancies/defect sites, SSA, and crystallite size which are controlled by pretreatment conditions.

4. Conclusions

The molecular structures of CeO_2 , which were treated under oxidizing and reducing conditions with varied temperatures (400, 500, and 700 °C), were investigated by BET, XRD, Raman spectroscopy, and XPS. The results from the XRD spectroscopy reveal that the pretreatment of the CeO_2 catalysts at higher temperatures caused an increase in the crystallinity and crystallite size. These changes were accompanied by a decrease in the surface area and defect sites, and an increase in the pore

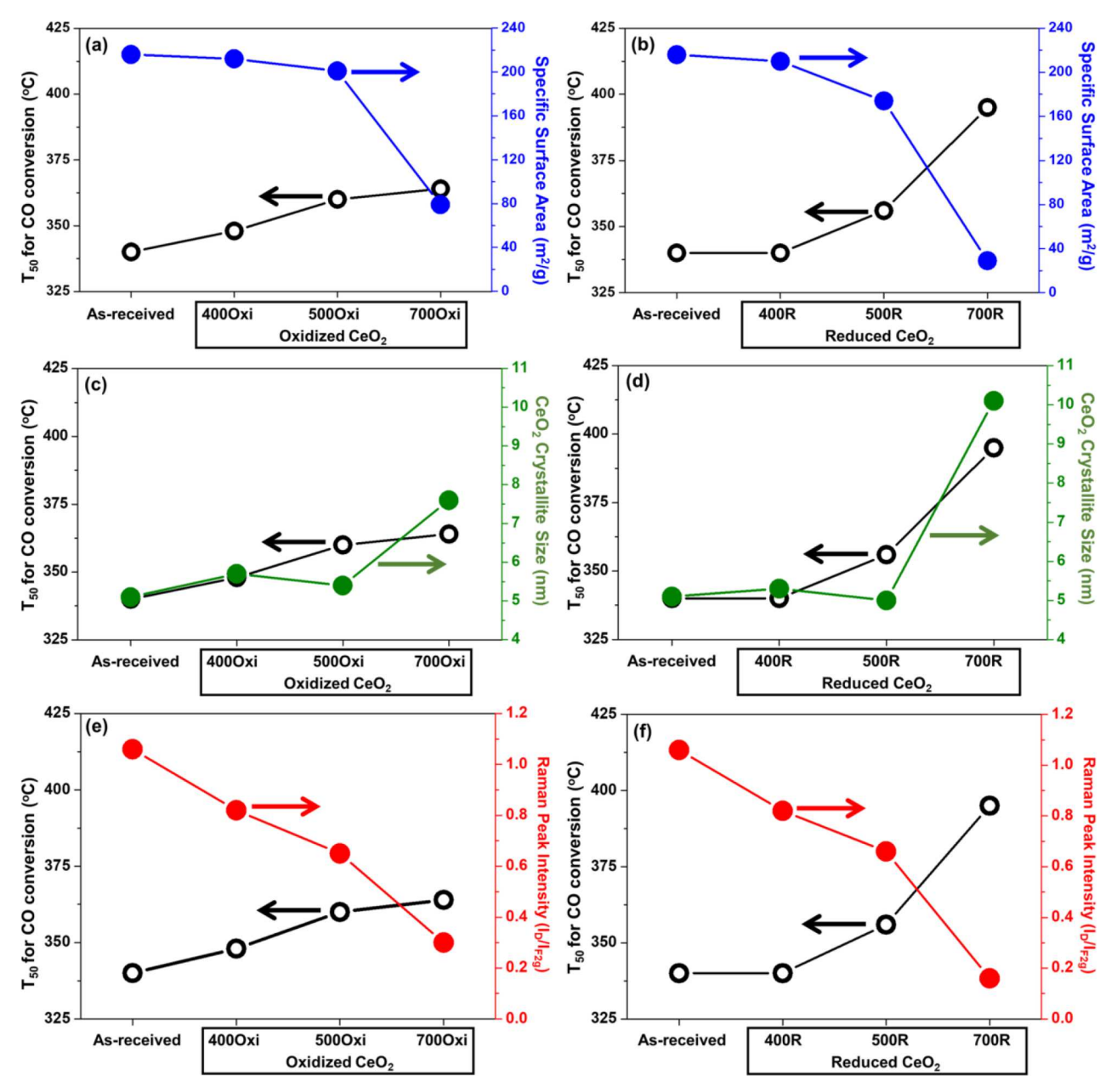


Fig. 8. T_{50} for CO conversion and Physical properties of as-received, oxidized, and reduced CeO₂ catalysts.

size as the pretreatment temperature increased. This most likely indicates slight sintering of the samples at high temperatures. The XPS showed an increase in the Ce³⁺ concentrations on the surface of the pretreated samples as compared to the as-received sample suggesting the thermal pretreatment can promote the generate of surface Ce³⁺ species. Catalytic activity results revealed that the overall catalytic performance (per gram basis) for both oxidized and reduced CeO₂ catalysts were decreased with increasing pretreatment temperature, especially at 700 °C. When comparing the CO conversion results of the oxidized and the reduced samples, it was seen that the oxidized samples had a slightly higher CO conversion than their reduced counterparts at the same temperature. The specific oxidation rate (μ mol_{CO}/s/m²) for the oxidized and reduced samples showed the highest value at 700 °C and was shown to be further improved by the reduction pretreatment. Overall, it can be noted that the temperature of the pretreatment has much more of an impact on the catalytic activity of the catalyst compared to the type of treatment (oxidation/reduction). The catalytic performances were mainly controlled by the physical properties, such as SSA, oxygen vacancies/defect sites, and crystallite size.

Author contributions

The manuscript was written through contributions of all authors. All authors have given approval to the final version of the manuscript.

CRediT authorship contribution statement

Kyung-Min Lee: Methodology, Formal analysis, Writing – original draft, Writing – review & editing. Melanie Brito: Formal analysis, Methodology, Writing – original draft, Writing – review & editing, Resources. Jamie DeCoster: Resources, Methodology, Formal analysis, Writing – original draft, Writing – review & editing. Kelvin Linskens: Resources, Methodology, Formal analysis, Writing – original draft, Writing – review & editing. Kelvin Linskens: Resources, Methodology, Formal analysis, Writing – original draft, Writing – review & editing. Won-Il Lee: Methodology, Formal analysis, Writing – review & editing. Emily Kim: Formal analysis, Writing – original draft, Writing – review & editing. Hajoon Kim: Formal analysis, Writing – original draft, Writing – review & editing. Chang-Yong Nam: Formal analysis, Writing – review & editing. Taejin Kim: Supervision, Writing – original draft, Writing – review & editing, Project administration, Funding acquisition.

Declaration of Competing Interest

The authors declare that they have no known competing financial interests or personal relationships that could have appeared to influence the work reported in this paper.

Acknowledgments

The authors acknowledge funding support from the National Science Foundation (NSF-CBET-2050824). The authors would also like to thank the Advanced Energy Research and Technology Center (AERTC) for the facilities at the Stony Brook University. This research used the beamline 28-ID-1 of the National Synchrotron Light Source II (NSLS-II) and the Materials Synthesis and Characterization Facility of Center for Functional Nanomaterials (CFN), which are U.S. Department of Energy (DOE) Office of Science User Facilities at Brookhaven National Laboratory under Contract No. DE-SC0012704.

Supplementary materials

Supplementary material associated with this article can be found, in the online version, at doi:10.1016/j.mcat.2022.112465.

References

- S. Royer, D. Duprez, Catalytic oxidation of carbon monoxide over transition metal oxides, ChemCatChem 3 (2011) 24–65, https://doi.org/10.1002/cctc.201000378.
- [2] J. Guzman, S. Carrettin, A. Corma, Spectroscopic evidence for the supply of reactive oxygen during CO oxidation catalyzed by gold supported on nanocrystalline CeO₂, J. Am. Chem. Soc. 127 (2005) 3286–3287, https://doi.org/ 10.1021/ia043755s
- [3] Y. Park, S.K. Kim, D. Pradhan, Y. Sohn, Surface treatment effects on CO oxidation reactions over Co, Cu, and Ni-doped and codoped CeO₂ catalysts, Chem. Eng. J. 250 (2014) 25–34, https://doi.org/10.1016/j.cej.2014.03.070.
- [4] D. Gamarra, C. Belver, M. Fernandez-Garcia, A. Martinez-Arias, Selective CO oxidation in excess H₂ over copper-ceria catalysts: identification of active entities/species, J. Am. Chem. Soc. 129 (2007) 12064–12065, https://doi.org/10.1021/ia0739366
- [5] J. Lin, X. Wang, T. Zhang, Recent progress in CO oxidation over Pt-group-metal catalyst at low temperatures, Chin. J. Catal. 37 (2016) 1805–1813, https://doi.org/ 10.1016/\$1872-2067(16)62513-5.
- [6] I. Langmuir, The mechanism of the catalytic action of platinum in the reactions 2CO+O₂=2CO₂ and 2H₂+O₂=2H₂O, J. Chem. Soc. Faraday Trans. 17 (1922) 621-654, https://doi.org/10.1039/TF9221700621.
- [7] M. Haruta, T. Kobayashi, H. Sano, N. Yamada, ChemInform abstract: novel gold catalysts for the oxidation of carbon monoxide at a temperature far below 0 °C, Prep. Org. Chem. 18 (1987), https://doi.org/10.1002/chin.198742098.
- [8] G. Germani, P. Alphonse, M. Courty, Y. Schuurman, C. Mirodatos, Platinum/ceria/ alumina catalysts on microstructures for carbon monoxide conversion, Catal. Today 110 (2005) 114–120, https://doi.org/10.1016/j.cattod.2005.09.017.
- [9] J. Yang, J. Guo, Y. Wang, T. Wang, J. Gu, L. Peng, N. Xue, Y. Zhu, X. Guo, W. Ding, Reduction-oxidation pretreatment enhanced catalytic performance of Co₃O₄/Al₂O₃ over CO oxidation, Appl. Surf. Sci. 453 (2018) 330–335, https://doi.org/10.1016/ j.apsusc.2018.05.103.
- [10] A. Bumajdad, S. Al-Ghareeb, M. Madkour, F. Al Sagheer, Non-noble, efficient catalysts of unsupported a-Cr₂O₃ nanoparticles for low temperature CO Oxidation, Sci. Rep. 7 (2017) 14788, https://doi.org/10.1038/s41598-017-14779-x.
- [11] P.R. Bueno, E.R. Leite, M.M. Oliveria, M.O. Orlandi, E. Longo, Role of oxygen at the grain boundary of metal oxide varistors: a potential barrier formation mechansim, Appl. Phys. Lett. 79 (2001) 48–50, https://doi.org/10.1063/1.1378051.
- [12] E.C. Lovell, A. Fuller, J. Scott, R. Amal, Enhancing Ni-SiO₂ catalysts for the carbon dioxide reforming of methane: reduction-oxidation-reduction pre-treatment, Appl. Catal. B Environ. 199 (2016) 155–165, https://doi.org/10.1016/j. apcatb.2016.05.080.
- [13] J.H. Jang, Y. Xu, M. Demura, D.M. Wee, T. Hirano, Catalytic activity improvement of Ni₃Al foils for methanol decomposition by oxidation-reduction pretreatment, Appl. Catal. A Gen. 398 (2011) 161–167, https://doi.org/10.1016/j. apcata.2011.03.040.
- [14] L.E. Gomez, I.S. Tiscornia, A.V. Boix, E.E. Miro, CO preferential oxidation on cordierite monoliths coated with Co/CeO₂ catalysts, Int. J. Hydrog. Energy 37 (2012) 14812–14819, https://doi.org/10.1016/j.ijhydene.2012.01.159.
- [15] M. Happel, J. Myslivecek, V. Johanek, F. Dvorak, O. Stetsovych, Y. Lykhach, V. Matolín, J. Libuda, Adsorption sites, metal-support interactions, and oxygen spillover identified by vibrational spectroscopy of adsorbed CO: a model study on Pt/ceria catalysts, J. Catal. 289 (2012) 118–126, https://doi.org/10.1016/j. icat.2012.01.022.
- [16] M. Kang, M.W. Song, C.H. Lee, Catalytic carbon monoxide oxidation over CoOx/ CeO₂ composite catalysts, Appl. Catal. A Gen. 251 (2003) 143–156, https://doi. org/10.1016/S0926-860X(03)00324-7.
- [17] M. Nolan, J.E. Fearon, G.W. Watson, Oxygen vacancy formation and migration, Solid State Ion. 177 (2006) 3069–3074, https://doi.org/10.1016/j. ssi 2006 07 045
- [18] C. Xu, X. Qu, Cerium oxide nanoparticle: a remarkably versatile rare earth nanomaterial for biological applications, NPG Asia Mater. 6 (2014), https://doi. org/10.1038/am.2013.88.
- [19] J. Kullgren, Oxygen Vacancy Chemistry in Ceria 896, Acta Universitatis Upsaliensis, 2012, p. 59.
- [20] H. Kim, H. Lee, G. Henkelman, CO oxidation mechanism on CeO₂-supported Au nanopartices, J. Am. Chem. Soc. 134 (2012) 1560–1570, https://doi.org/10.1021/ i>207510v
- [21] Y. Lou, Y. Cai, W. Hu, L. Wang, Q. Dai, W. Zhan, Y. Guo, P. Hu, X. Cao, J. Liu, Y. Guo, Identification of active area as active center for CO oxidation over single Au atom catalyst, ACS Catal. 10 (2020) 6094–6101, https://doi.org/10.1021/poperate/10.0123/
- [22] Y. Lou, J. Xu, Y. Zhang, C. Pan, Y. Dong, Y. Zhu, Metal-support interaction for heterogeneous catalysis: from nanoparticles to single atoms, Mater. Today Nano 12 (2020), 100093, https://doi.org/10.1016/j.mtnano.2020.100093.
- [23] W. Wang, W. Yu, P. Du, H. Xu, Z. Jin, R. Si, C. Ma, S. Shi, C. Jia, C. Yan, Crystal plane effect of ceria on supported copper oxide cluster catalyst for CO oxidation: importance of metal-support interaction, ACS Catal. 7 (2017) 1313–1329, https://doi.org/10.1021/acscatal.6b03234.
- [24] E. Aneggi, J. Llorca, M. Boaro, A. Trovarelli, Surface-structure sensitivity of CO oxidation over polycrystalline ceria powders, J. Catal. 234 (2005) 88–95, https://doi.org/10.1016/j.jcat.2005.06.008.
- [25] K. Wang, Y. Chang, L. Lv, Y. Long, Effect of annealing temperature on oxygen vacancy concentrations of nanocrystalline CeO₂ film, J. Appl. Surf. Sci. 351 (2015) 164–168, https://doi.org/10.1016/j.apsusc.2015.05.122.

- [26] M. Konsolakis, M. Lykaki, Facet-dependent reactivity of ceria nanoparticles exemplified by CeO₂-based transition metal catalyst: a critical review, Catalysts 11 (2021) 452, https://doi.org/10.3390/catal11040452.
- [27] X. Zheng, Y. Li, L. Zhang, L. Shen, Y. Xiao, Y. Zhang, C. Au, L. Jiang, Insight into the effect of morphology on catalytic performance of porous CeO₂ nanocrystals for H₂S selectivity oxidation, Appl. Catal. B Environ. 252 (2019) 98–110, https://doi.org/ 10.1016/j.apcatb.2019.04.014.
- [28] F.M. Pinto, V.Y. Suzuki, R.C. Silva, F.A. La Porta, Oxygen defects and surface chemistry of reducible oxides, Front. Mater. 6 (2019) 1–15, https://doi.org/ 10.3389/fmats.2019.00260.
- [29] C. Prescher, V.B. Prakapenda, DIOPTAS: a program for reduction of twodimensional X-ray diffraction data and data exploration, High Press. Res. 35 (2015) 223–230, https://doi.org/10.1080/08957959.2015.1059835.
- [30] G. Jayakumar, A. Irudayaraj, D. Raj, Particle size effect on the properties of cerium oxide (CeO₂) nanoparticles synthesized by hydrothermal method, Mech. Mater. Sci. Eng. 9 (2017), https://doi.org/10.2412/mmse.3.4.481.
- [31] G. Basina, K. Polychronopoulou, A.F. Zedan, K. Dimos, M.S. Katsiotis, A. P. Fotopoulos, I. Ismail, V. Tzitzios, Ultrasmall metal-doped CeO₂ nanoparticles for low-temperature CO oxidation, ACS Appl. Nano Mater. 3 (2020) 10805–10813, https://doi.org/10.1021/acsanm.0c02090.
- [32] E. Özkan, P. Cop, F. Benfer, A. Hofmann, M. Votsmeier, J.M. Guerra, M. Giar, C. Heiliger, H. Over, B.M. Smarsly, Rational synthesis concept for cerium oxide nanoparticles: on the impact of particle size on the oxygen storage capacity, J. Phys. Chem. 124 (2020) 8736–8748, https://doi.org/10.1021/acs.jpcc.0c00010.
- [33] K. Berent, S. Komarek, R. Lach, W. Pyda, The effect of calcination temperature on the structure and performance of nanocrystalline mayenite powders, Materials 12 (2019) 3476, https://doi.org/10.3390/ma12213476.
- [34] L. Bourja, B. Bakiz, A. Benlhachemi, M. Ezahri, S. Villain, J.R. Gavarri, Synthesis and characterization of nanosized Ce_{1-x}bi_xO₂₋₆ solid solutions for catalytic applications, J. Taibah Univ. Sci. 4 (2010) 1–8, https://doi.org/10.1016/S1658-3655(12)60021-1
- [35] Z. Wang, F. Lin, S. Jiang, K. Qiu, M. Kuang, R. Whiddon, K. Cen, Ceria substrate-oxide composites as catalyst for highly efficient catalytic oxidation of NO by O₂, Fuel 166 (2016) 352–360, https://doi.org/10.1016/j.fuel.2015.11.012.
- [36] X. Zhang, K. Li, W. Shi, C. Wei, Z. Song, S. Yang, Z. Sun, Baize-like CeO₂ and NiO/CeO₂ nanorod catalysts prepared by dealloying for CO oxidation, Nanotechnology 28 (2017) 1–11. https://doi.org/10.1088/1361-6528/28/4/0.45602.
- [37] M. Thommes, K. Kaneko, A.V. Neimark, J.P. Olivier, F. Rodriguez-Reinoso, J. Rouquerol, K.S.W. Sing, Physisorption of gases, with special reference to the evaluation of surface area and pore size distribution (IUPAC technical report), Pure Appl. Chem. (2015) 1–19, https://doi.org/10.1515/pac-2014-1117.
- [38] K. Lee, G. Kwon, S. Hwang, J.A. Boscoboinik, T. Kim, Investigation of NO reduction by CO reaction over oxidized and reduced NiOx/CeO₂ catalysts, Catal. Sci. Technol. 11 (2021) 7850–7865, https://doi.org/10.1039/D1CY01215K.
- [39] M. Thommes, Physical adsorption characterization of nanoporous materials, Chem. Ing. Tech. 82 (2010) 1059–1073, https://doi.org/10.1002/cite.201000064.
- [40] R. Schmitt, A. Nenning, O. Kraynis, R. Korobko, A.I. Frenkel, I. Lubomirsky, S. M. Haile, J.L.M. Rupp, A review of defect structure and chemistry in ceria and its solid solutions, Chem. Soc. Rev. 49 (2020) 554–592, https://doi.org/10.1039/c0cs0588a
- [41] Z. Wu, M. Li, S.H. Overbury, On the structure dependence of CO oxidation over CeO₂ nanocrystals with well-defined surface planes, J. Catal. 285 (2012) 61–73, https://doi.org/10.1016/j.jcat.2011.09.011.
- [42] M.N.S.M. Idris, H. Chiang, N. Muslim, Y.C. Chau, A.H. Mahadi, N.Y. Voo, C.M. Lim, A comparative study of visible raman scattering of ceria prepared by sol-gel and hydrothermal techniques with gold nanoparticles, IOP Conf. Ser. Mater. Sci. Eng. 409 (2018), 012012, https://doi.org/10.1088/1757-899x/409/1/012012.

- [43] M. Mogensen, N.M. Sammes, G.A. Tompsett, Physical, chemical and electrochemical properties of pure and doped ceria, Solid State Ion. 129 (2000) 63–94, https://doi.org/10.1016/S0167-2738(99)00318-5.
- [44] T. Hattori, K. Kobayashi, M. Ozawa, Size effect of Raman scattering on CeO₂ nanocrystal by hydrothermal method, Jpn. J. Appl. Phys. 56 (2017), https://doi.org/10.7567/jjap.56.01ae06, 01AE06-1-6.
- [45] E. Sartoretti, C. Novara, F. Giorgis, M. Piumetti, S. Bensaid, N. Russo, D. Fino, In situ Raman analyses of the soot oxidation reaction over nanostructured ceria-based catalysts, Sci. Rep. 9 (2019) 1–14, https://doi.org/10.1038/s41598-019-39105-5.
- [46] D. Prieur, W. Bonani, K. Popa, O. Walter, K.W. Kriegsman, M.H. Engelhard, X. Guo, R. Eloirdi, T. Gouder, A. Beck, T. Vitova, A.C. Scheinost, K. Kvashnina, P. Martin, Size dependence of lattice parameter and electronic structure in CeO₂ nanoparticles, Inorg. Chem. 59 (2020) 5760–5767, https://doi.org/10.1021/acs.inorgchem.0c00506.
- [47] T. Taniguchi, T. Watanabe, N. Sugiyama, A. Subramani, H. Wagata, N. Matsushita, M. Yoshimura, Identifying defects in Ceria-based nanocrystals by UV resonance raman spectroscopy, J. Phys. Chem. 113 (2009) 19789–19793, https://doi.org/ 10.1021/ip9049457.
- [48] S. Tsunekawa, R. Sivamohan, S. Ito, A. Kasuya, T. Fukuda, Structural study on monosize CeO_{2-x} nano-particles, Nanostruct. Mater. 11 (1999) 141–147, https://doi.org/10.1016/S0965-9773(99)00027-6.
- [49] S. Tsunekawa, T. Fukuda, A. Kasuya, Blue shift in ultraviolet absorption spectra of monodisperse nanoparticles, Int. J. Appl. Phys. 87 (2000) 1318–1321, https://doi. org/10.1063/1.372016.
- [50] L. Chen, Z.H. Si, X.D. Wu, D. Weng, DRIFT study of CuO-CeO₂-TiO₂ mixed oxides for NO_x reduction with NH₃ at low temperatures, ACS Appl. Mater. Interfaces 6 (2014) 8134–8145, https://doi.org/10.1021/am5004969.
- [51] C. Deng, Q. Huang, X. Zhu, Q. Hu, W. Su, J. Qian, L. Dong, B. Li, M. Fan, C. Liang, The influence of Mn-doped CeO₂ on the activity of CuO/CeO₂ in CO oxidation and NO+ CO model reaction, Appl. Surf. Sci. 389 (2016) 1033–1049, https://doi.org/ 10.1016/j.apsusc.2016.08.035.
- [52] Z. Wu, M. Li, J. Howe, H.M. Meyer, S.H. Overbury, Probing defect sites on CeO₂ nanocrystals with well-defined surface planes by raman spectroscopy and O₂ adsorption, Langmuir 26 (2010) 16595–16606, https://doi.org/10.1021/la101723w.
- [53] M. Baudin, M. Wojcik, K. Hermansson, Dynamics, structure and energetics of the (111), (011) and (001) surfaces of ceria, Surf. Sci. 468 (2000) 51–61, https://doi. org/10.1016/S0039-6028(00)00766-4.
- [54] M. Piumetti, T. Andana, S. Bensaid, N. Russo, D. Fino, R. Pirone, Study on the CO oxidation over ceria-based nanocatalysts, Nanoscale Res. Lett. 11 (2016) 1–8, https://doi.org/10.1186/s11671-016-1375-z.
- [55] M. Li, A.C. van Veen, Tuning the catalytic performance of Ni-catalysed dry reforming of methane and carbon deposition via Ni-CeO_{2-x} interaction, Appl. Catal. B Environ. 237 (2018) 641–648, https://doi.org/10.1016/j.apcatb.2018.06.032.
- [56] S. Zhang, J. Lee, D.H. Kim, T. Kim, NO reduction by CO over CoO_x/CeO₂ catalysts: effect of support calcination temperature on activity, Mol. Catal. 482 (2020), 110703, https://doi.org/10.1016/j.mcat.2019.110703.
- [57] J.R. McBride, K.C. Hass, B.D. Poindexter, W.H. Weber, Raman and x-ray studies of Ce_{1-x}RE_xO_{2-y}, where RE = La, Pr, Nd, Eu, Gd, and Tb, J. Appl. Phys. 76 (1994) 2435–2441, https://doi.org/10.1063/1.357593.
- [58] T. Divya, C. Anjali, K.R. Sunajadevi, K. Anas, N.K. Renuka, Influence of hydrothermal synthesis conditions on lattice defects in cerium oxide, J. Solid State Chem. 300 (2021), https://doi.org/10.1016/j.jssc.2021.122253, 122253 (1-9).
- [59] M. Guo, J. Lu, Y. Wu, Y. Wang, M. Luo, UV and visible raman studies of oxygen vacancies in rare-earth-doped Ceria, Langmuir 27 (2011) 3872–3877, https://doi. org/10.1021/la200292f.

Support Information

Influence of oxidizing and reducing pretreatment on the catalytic performance of CeO₂ for CO oxidation

Kyung-Min Lee¹, Melanie Brito¹, Jamie DeCoster¹, Kelvin Linskens¹, Kareem Mehdi¹, Won-Il Lee¹, Emily Kim², Hajoon Kim³, Gihan Kwon⁴, Chang-Yong Nam^{1,5}, Taejin Kim^{1,*}

⁵ Center for Functional Nanomaterials, Brookhaven National Laboratory, Upton, NY, 11973, U.S.A

Corresponding Author: * TJK: Materials Science and Chemical Engineering Department, Stony Brook University, Stony Brook, NY 11794, taejin.kim@stonybrook.edu

¹ Materials Science and Chemical Engineering Department, Stony Brook University, Stony Brook, NY, 11794, U.S.A

² Hankuk Academy of Foreign Studies, Yongin, Gyeonggi-do, KS009, South Korea

³ Radnor Senior High School, Radnor, PA, 19087, U.S.A

⁴ National Synchrotron Light Source II, Brookhaven National Laboratory, Upton, NY 11973, U.S.A

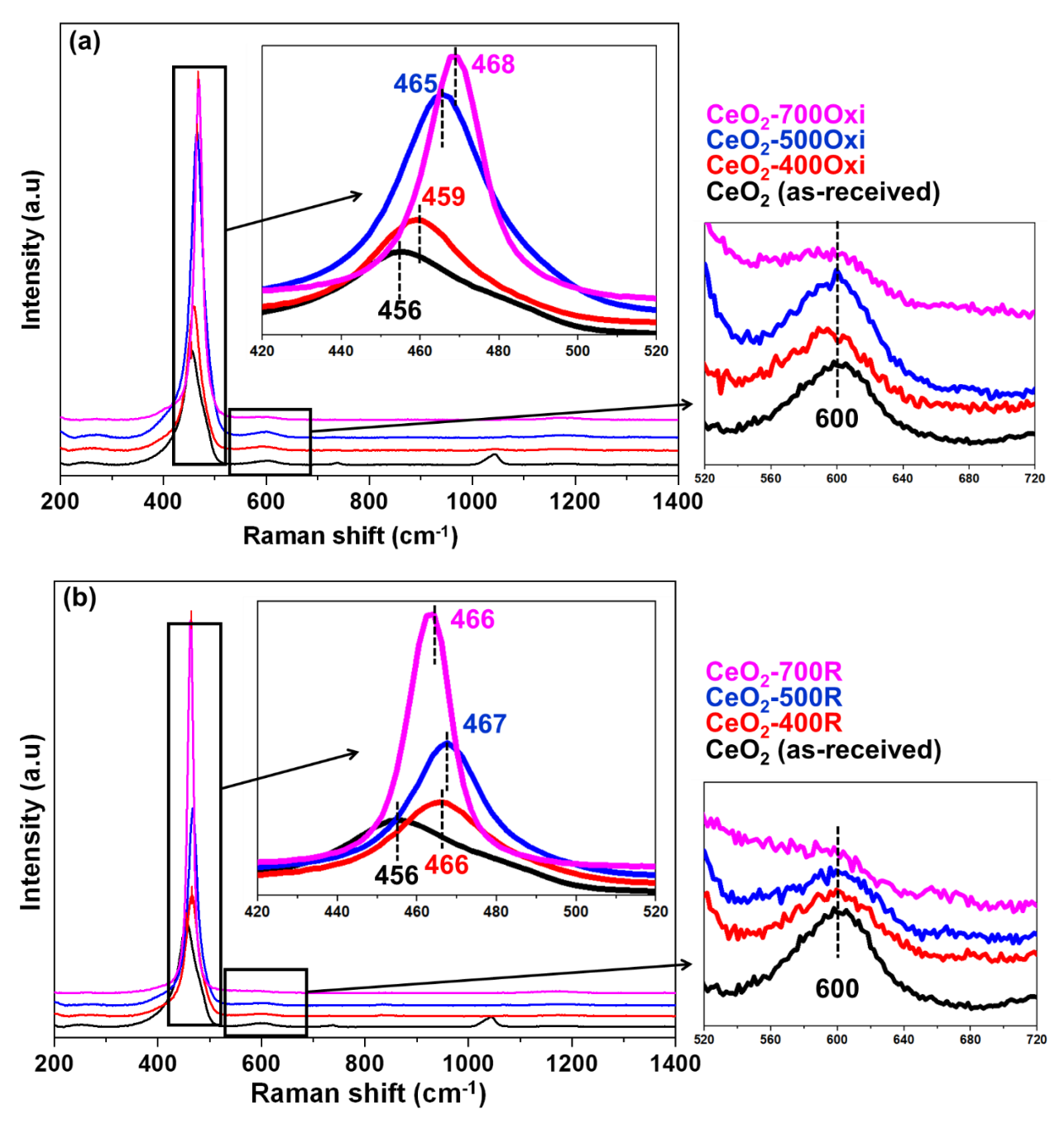


Figure S1: Visible Raman spectra of (a) ceria treated with air (oxidized) (b) ceria treated with hydrogen (reduced)

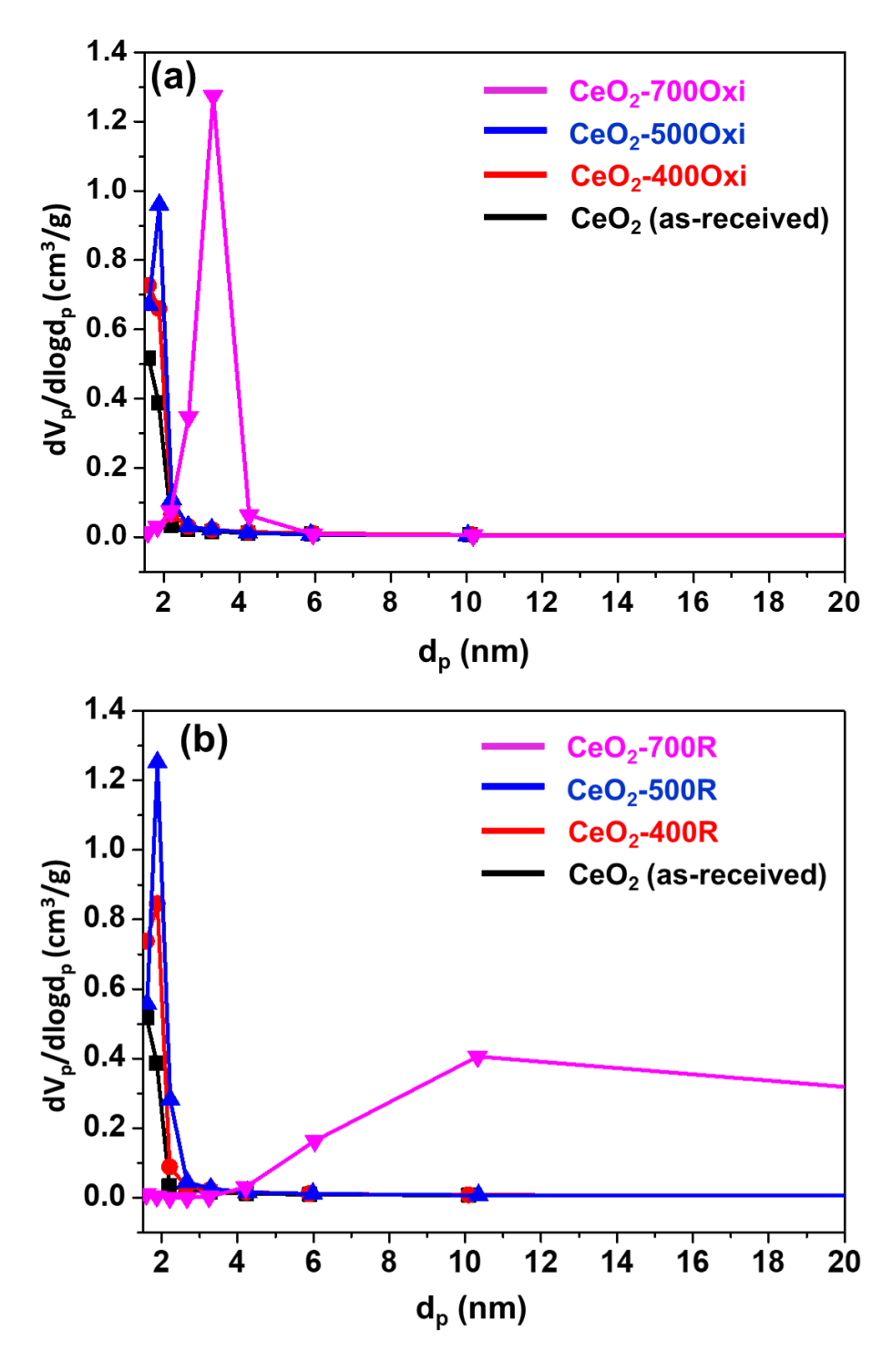


Figure S2: Pore size distributions of the (a) ceria treated with air (oxidized) and (b) ceria treated with hydrogen (reduced) (calculated with the desorption branch with BJH method)